Available online at www.sciencedirect.com
ScienceDirect
International Journal of Heat and Mass Transfer 50 (2007) 4117–4130
International Journal of HEAT and MASS TRANSFER
www.elsevier.com/locate/ijhmt

Estimation of time-dependent heat flux and measurement bias in two-dimensional inverse heat conduction problems

Umer Zeeshan Ijaz [a], Anil Kumar Khambampati [a], Min-Chan Kim [b], Sin Kim [c], Kyung-Youn Kim [a,*]

[a] Department of Electrical and Electronic Engineering, Cheju National University, Cheju 690-756, South Korea
[b] Department of Chemical Engineering, Cheju National University, Cheju 690-756, South Korea
[c] Department of Nuclear and Energy Engineering, Cheju National University, Cheju 690-756, South Korea

Received 27 August 2006; received in revised form 27 February 2007
Available online 9 May 2007

Abstract

This paper presents the results from the adaptive estimator developed to estimate time-dependent boundary heat flux in two-dimensional heat conduction domain with heated and insulated walls. For the estimation, the algorithm requires only the temperatures measured at the insulated walls. In addition, the estimator also predicts the bias in the measurements. In modeling the system, it is assumed that the input flux and bias sequence dynamics can be modeled by a semi-Markov process. By incorporating the semi-Markovian concept into a Bayesian estimation technique, the estimator consists of a bank of parallel, adaptively weighted, Kalman filters. Computer simulation results reveal that the proposed adaptive estimator has improved estimation performance even for step changing heat flux and measurement bias.

Keywords: Adaptive estimation; Kalman filter; Inverse heat conduction problems; Recursive least square estimation; Measurement bias

1. Introduction

The inverse heat conduction problem (IHCP) has received much attention in recent years since it has been widely used in practical engineering problems involving the estimation of surface conditions or initial conditions as well as thermal properties of a body from known information like temperatures measured at the prescribed positions. There exist many methods to solve the IHCP and the majority of researchers use the approaches where the unknowns are determined to minimize the sum of squares of the differences between the measured and the computed temperatures at the selected spatial and/or temporal points (refer to Kim et al. [1]). In general, the approaches adopt the iterative scheme and the regularizations are implemented to mitigate the ill-posedness of IHCP.

The Kalman filter estimation method is successfully used in predicting one-dimensional, two-dimensional, multidimensional and nonlinear IHCP. There have been attempts to solve one-dimensional inverse heat transfer problems by Scarpa and Milano [2] and Kaipio and Somersalo [3]. In recent years, many applications appeared in which Kalman filter has been used in conjunction with recursive-least square algorithm (RLSA), for example the work of Tuan et al. [4–11], deals with one-dimensional and two-dimensional problems. Extending that work, recently, Jang et al. [12] has attempted to use a RLSA based on the Kalman filter to estimate the boundary heat flux varying impulsively with time by employing the finite-element scheme instead of finite-difference scheme [4] to discretize the problem in space, allowing multidimensional problems of various geometries to be treated. For

* Corresponding author. Tel.: +82 64 754 3664; fax: +82 64 756 1745.
E-mail address: kyungyk@cheju.ac.kr (K.-Y. Kim).

0017-9310/$ - see front matter © 2007 Elsevier Ltd. All rights reserved.
doi:10.1016/j.ijheatmasstransfer.2007.02.037

Nomenclature

c_0	uniform initial temperature
C	scale factor
H	measurement matrix
I	identity matrix
k	time(discretized)
K	Kalman gain
K_b	gain
M, N	total number of spatial nodes
O, P	number of filters
Pe	filter's error covariance matrix
P_b	error covariance matrix
q	heat flux
$q^{(i)}$	discrete range of heat flux
Q	process noise covariance matrix
Q_b	input flux covariance matrix
R	measurement noise covariance matrix
R_b	measurement bias covariance matrix
t	time
t_f	final time
T	temperature
Δt	sampling interval
w	process noise vector
W	weight matrix
x, y	dimensionless axial coordinate
x_s, y_s	measurement location
X	state vector
Z	observation vector
Γ	input matrix
δ	Kronecker delta
υ	measurement noise vector
$\upsilon^{(j)}$	discrete range for measurement bias
υ_b	measurement bias
o	null matrix
σ	standard deviation
Φ	state transition matrix
ψ_1, ψ_2, ψ_3	submatrices of Ψ
Ψ	coefficient matrix
ω_1, ω_2	submatrices of Ω
Ω	coefficient matrix
θ_q	Markov transition matrix for heat flux
θ_υ	Markov transition matrix for measurement bias
α	first-order low-pass filter parameter
$\hat{}$	estimated
$-$	estimated by filter
T	transpose of a matrix
α, β	indices
i, j	indices

higher dimension problems, the straight forward implementation of the Kalman filter becomes difficult as the size of covariance equation increases. Therefore, one of the most important prerequisites for the successful implementation of a Kalman filter for the purpose of real-time estimation is the development of a reliable low dimensional model, hence, dimension reduction techniques like Karhunen–Loéve Galerkin procedure is used with Kalman filter by Park and Jung [13] for solving multidimensional heat conduction problems. For the case of nonlinear IHCP, extended version of discrete Kalman filter have been used by Daouas and Radhouani [14,15] to nonlinear IHCP to estimate surface heat flux density.

It is noteworthy that Tuan et al. [4] developed a RLSA based on the Kalman filter for two-dimensional IHCP to estimate the boundary heat flux varying impulsively with time. Their approach gives good estimates for estimating unknown heat sources or heat flux inputs on the boundaries. In some of their papers [7,8], they have proposed improvement in Kalman filter with RLSA approach by having RLSA weighted by forgetting factor to robustly extract the unknowns. The maximum likelihood type estimator (M-estimator) combined with Huber psi-function is used to construct the weighting forgetting factor. In the context of forgetting factor, Wang et al. [16] proposed extended Kalman filter with RLSA weighted by forgetting factor to estimate nonlinear heat conduction problems.

However sometimes in real situations, in addition to measurement noise, the sensors might also have sensor bias i.e., it is known that the environment around the measurement devices may introduce an unknown bias term in the measurement sequence or failures in system measurement instrumentation may randomly occur. Scarpa and Milano [17] considers the effect of random noises superposed onto the measurement signals, the bias arising from the calibration of sensors for the IHCP. They conceive the calibration process as an integral part of the experiment to quantify the effect of the bias to obtain the better estimates. Because of the presence of sensor bias, the input estimation with RLSA algorithm does not seem to converge well to the true estimates and hence one must resort to alternatives, for instance, Bayesian computation technique. The Bayesian computational technique has many advantages as it is able to quantify system uncertainty and random data error, to derive a probabilistic description of the inverse solution, to provide extensive spatial/temporal regularization to the ill-posedness of the inverse problem, and to allow adaptive sequential estimation. Wang and Zabaras in [18–21] developed a computational framework that integrates computational mathematics, Bayesian statistics, statistical computation, and reduced-order modeling to address data-driven inverse heat and mass transfer problems.

In the context of measurement sensor bias, the present work addresses an adaptive state estimator based on

Kalman filter to estimate the temporal heat flux of a two-dimensional heat conduction medium using the measured temperatures from two sensors. In modeling the system, it is assumed that the input flux and bias sequence dynamics can be modeled by a semi-Markov process. The adaptive state estimator (ASE) is based on Moose et al. [22] in which they developed an adaptive state estimator for passive underwater tracking of maneuvering targets. The resulting adaptive estimator is an on-line estimator which estimates temperature distribution, input heat flux and the measurement bias together when the new measurements become available and hence like other Kalman-type filters, it does not require the saving of prior measurements. It is worth mentioning here that Kim et al. [23] has applied ASE based on Moose et al. [24] to one-dimensional IHCP for estimation of input heat flux. Extending that work and considering measurement bias into account, we have focused our research on a typical two-dimensional heat

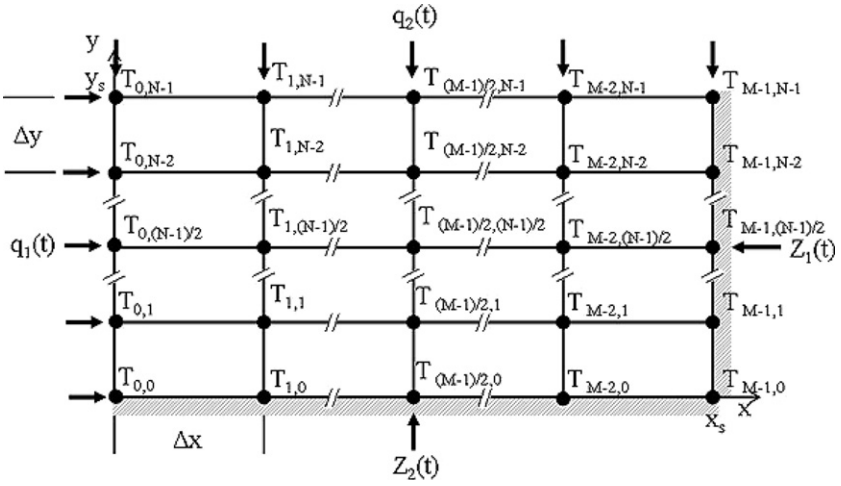

Fig. 1. Two-dimensional inverse heat conduction problem considered.

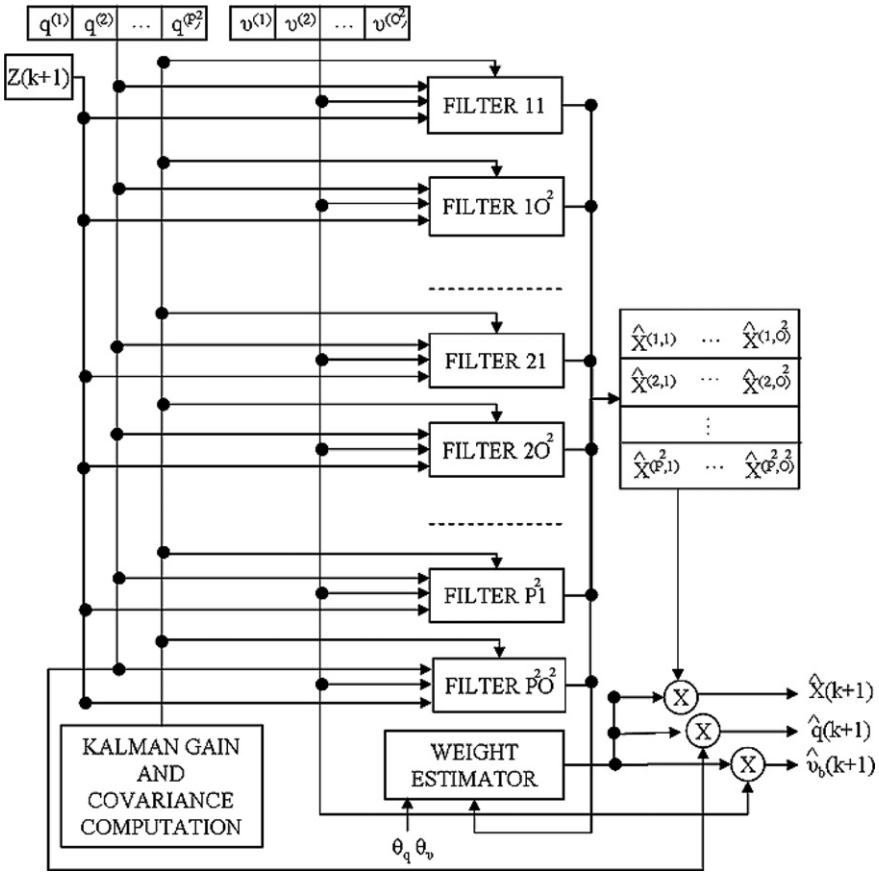

Fig. 2. Block diagram of adaptive estimator.

conduction problem. This study shows that ASE consisting of Kalman filters connected in parallel gives good performance in the presence of measurement bias. Each filter has its operating bound limiting the range of the unknown input heat flux and measurement bias.

2. Problem formulation

Let us consider a two-dimensional rectangular region, $0 \leqslant x \leqslant x_s,\ 0 \leqslant y \leqslant y_s$, initially at temperature $T(x,y,0)$. For times $t > 0$ the boundaries at $x = x_s$ and $y = 0$ are kept insulated, the temperature measurements $Z_1(t)$ and $Z_2(t)$ are known, and we need to estimate two input heat fluxes $q_1(t)$ and $q_2(t)$ acting on the surface $x = 0$ and $y = y_s$, respectively. Fig. 1 illustrates the heat conduction problem considered along with boundary and initial conditions. The governing equations in dimensionless form are given by

$$\frac{\partial T}{\partial t} = \frac{\partial^2 T}{\partial x^2} + \frac{\partial^2 T}{\partial y^2} \quad 0 \leqslant x \leqslant x_s,\ 0 \leqslant y \leqslant y_s \tag{1}$$

$$T(x,y,0) = c_0 \quad 0 \leqslant x \leqslant x_s,\ 0 \leqslant y \leqslant y_s \tag{2}$$

$$\frac{\partial T}{\partial x} = -q_1(t) \quad x = 0,\ 0 \leqslant y \leqslant y_s,\ t > 0 \tag{3}$$

$$\frac{\partial T}{\partial y} = 0 \quad 0 \leqslant x \leqslant x_s,\ y = 0,\ t > 0 \tag{4}$$

$$\frac{\partial T}{\partial x} = 0 \quad x = x_s,\ 0 \leqslant y \leqslant y_s,\ t > 0 \tag{5}$$

$$\frac{\partial T}{\partial y} = -q_2(t) \quad 0 \leqslant x \leqslant x_s,\ y = y_s,\ t > 0 \tag{6}$$

$$Z_1(t) = T\left(x_s, \frac{1}{2}y_s, t\right) + \upsilon_1(t) \quad x = x_s,\ y = \frac{1}{2}y_s,\ t > 0 \tag{7}$$

$$Z_2(t) = T\left(\frac{1}{2}x_s, 0, t\right) + \upsilon_2(t) \quad x = \frac{1}{2}x_s,\ y = 0,\ t > 0, \tag{8}$$

where c_0 is the uniform initial temperature, $q_1(t)$ and $q_2(t)$ are the unknown heat flux inputs to be estimated, and $Z_1(t)$ and $Z_2(t)$ are the noise-corrupted measurements, with $\upsilon_1(t)$ and $\upsilon_2(t)$ being the measurement noises assumed zero mean and white Gaussian. To formulate the relationship between temperature and boundary condition, a central finite-difference approximation for the space derivative is employed. Eq. (1) becomes

$$\begin{aligned}\dot{T}_{i,j}(t) &= \frac{T_{i+1,j}(t) - 2T_{i,j}(t) + T_{i-1,j}(t)}{\Delta x^2} + \frac{T_{i,j+1}(t) - 2T_{i,j}(t) + T_{i,j-1}(t)}{\Delta y^2} \\ &= \frac{1}{\Delta x^2}T_{i-1,j}(t) + \frac{1}{\Delta y^2}T_{i,j-1}(t) - \left(\frac{2}{\Delta x^2} + \frac{2}{\Delta y^2}\right)T_{i,j}(t) + \frac{1}{\Delta y^2}T_{i,j+1}(t) + \frac{1}{\Delta x^2}T_{i+1,j}(t)\end{aligned} \tag{9}$$

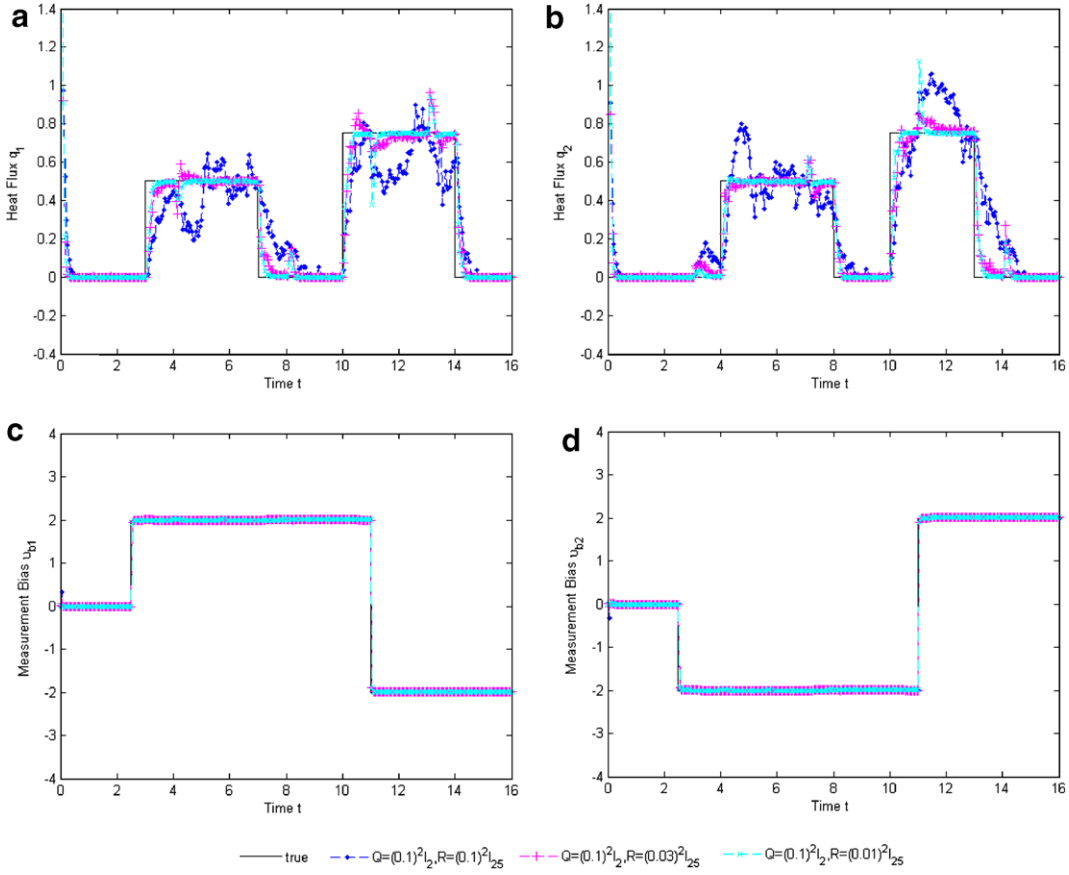

Fig. 3. Reconstructed heat fluxes and measurement biases for scenario 1. Parameters are $x_s = 0.5$, $y_s = 0.5$, $\Delta t = 0.005$, $Q_b = 0.001I_2$, $R_b = 0.001I_2$, $\alpha = 0.7$, $\theta^{(i,i)} = 0.95$, and $Pe(-1 \mid -1) = 10^{10}I_{25}$.

for $i = 1, \ldots, M-2$, $j = 1, \ldots, N-2$, and $M, N > 1$, where M and N are the total number of spatial nodes set up by odd number for x and y directions, respectively, and $\Delta x = x_s/(M-1)$ and $\Delta y = y_s/(N-1)$ are the space intervals. Note that the system state notation is defined as $T_{i,j}(t) = T(x_i, y_j, t)$. At the boundary $x = 0$, $T_{-1,j}(t)$ can be solved by using Eq. (3) as

$$\frac{\partial T_{0,j}(t)}{\partial x} = \frac{T_{1,j}(t) - T_{-1,j}(t)}{2\Delta x} = -q_1(t) \tag{10}$$

yielding

$$T_{-1,j}(t) = T_{1,j}(t) + 2\Delta x q_1(t) \tag{11}$$

Similarly, at the boundary at $y = 0$, $x = x_s$ and $y = y_s$ can be solved by using Eqs. (4) and (5), respectively, to get

$$T_{i,-1}(t) = T_{i,1}(t) \tag{12}$$

$$T_{M,j}(t) = T_{M-2,j}(t) \tag{13}$$

$$T_{i,N}(t) = T_{i,N-2}(t) + 2\Delta y q_2(t) \tag{14}$$

From Eqs. (12)–(14) and associated with fictitious process noise inputs [26], the continuous-time state equation can be written as

$$\dot{T}(t) = \Psi T(t) + \Omega[q(t) + w(t)], \tag{15}$$

where $w(t)$ is the process noise. This additional term represents the cumulative effects of uncertainty caused by modeling errors [27]. Moreover, the state vector $T(t) \in \mathbb{R}^{(M\times N)\times 1}$ is given by

$$T(t) = [T_0(t)T_1(t)\cdots T_{M-2}(t)T_{M-1}(t)]^{\mathrm{T}} \tag{16}$$

where

$$\begin{aligned} T_0(t) &= [T_{0,0}(t)T_{0,1}(t)\cdots T_{0,N-2}(t)T_{0,N-1}(t)\\ T_1(t) &= [T_{1,0}(t)T_{1,1}(t)\cdots T_{1,N-2}(t)T_{1,N-1}(t)\\ &\vdots\\ T_{M-1}(t) &= [T_{M-1,0}(t)T_{M-1,1}(t)\cdots T_{M-1,N-2}(t)T_{M-1,N-1}(t) \end{aligned} \tag{17}$$

The coefficient matrix $\Psi \in \mathbb{R}^{(M\times N)\times(M\times N)}$ is given by

$$\Psi = \begin{bmatrix} \psi_1 & \psi_3 & o & o & o & \cdots & o \\ \psi_2 & \psi_1 & \psi_2 & o & o & \cdots & o \\ o & \psi_2 & \psi_1 & \psi_2 & o & \cdots & o \\ \vdots & & & \ddots & & & \vdots \\ o & \cdots & o & \psi_2 & \psi_1 & \psi_2 & o \\ o & \cdots & o & o & \psi_2 & \psi_1 & \psi_2 \\ o & \cdots & o & o & o & \psi_3 & \psi_1 \end{bmatrix} \tag{18}$$

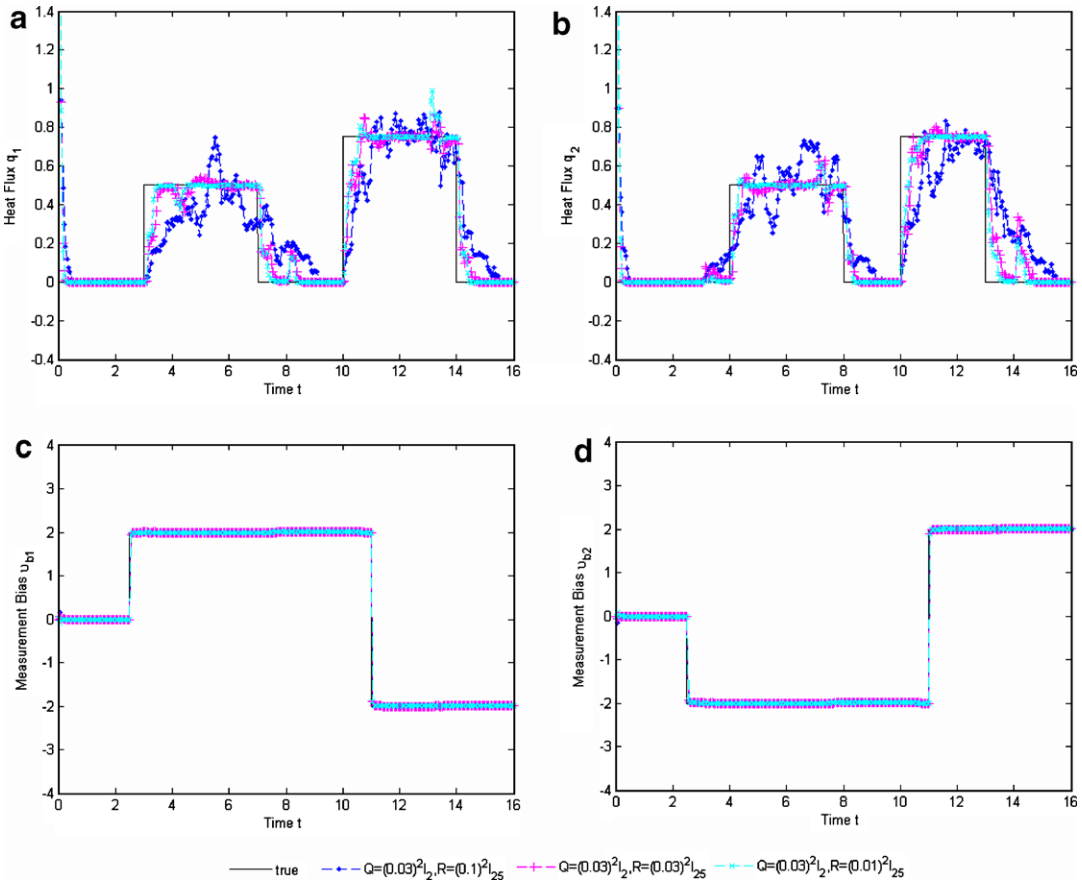

Fig. 4. Reconstructed heat fluxes and measurement biases for scenario 1. Parameters are $x_s = 0.5$, $y_s = 0.5$, $\Delta t = 0.005$, $Q_b = 0.001I_2$, $R_b = 0.001I_2$, $\alpha = 0.7$, $\theta^{(i,i)} = 0.95$, and $Pe(-1|-1) = 10^{10}I_{25}$.

in which

$$\psi_1 = \begin{bmatrix} -\left(\frac{2}{\Delta x^2}+\frac{2}{\Delta y^2}\right) & \frac{2}{\Delta y^2} & 0 & \cdots & 0 \\ \frac{1}{\Delta y^2} & -\left(\frac{2}{\Delta x^2}+\frac{2}{\Delta y^2}\right) & \frac{1}{\Delta y^2} & \cdots & 0 \\ \vdots & \ddots & \ddots & \ddots & \vdots \\ 0 & \cdots & \frac{1}{\Delta y^2} & -\left(\frac{2}{\Delta x^2}+\frac{2}{\Delta y^2}\right) & \frac{1}{\Delta y^2} \\ 0 & \cdots & 0 & \frac{2}{\Delta y^2} & -\left(\frac{2}{\Delta x^2}+\frac{2}{\Delta y^2}\right) \end{bmatrix}$$

$$\psi_2 = \begin{bmatrix} \frac{1}{\Delta x^2} & 0 & 0 & \cdots & 0 \\ 0 & \frac{1}{\Delta x^2} & 0 & & 0 \\ \vdots & & \ddots & & \vdots \\ 0 & \cdots & 0 & \frac{1}{\Delta x^2} & 0 \\ 0 & \cdots & 0 & 0 & \frac{1}{\Delta x^2} \end{bmatrix}, \quad \psi_3 = 2\psi_2 \tag{19}$$

The submatrices ψ_1, ψ_2, ψ_3 and o are $\mathbb{R}^{N\times N}$, where o is a null submatrix. The input matrix $\Omega \in \mathbb{R}^{(M\times N)\times 2}$ is given by

$$\Omega = \begin{bmatrix} \omega_1 \\ \omega_2 \\ \omega_2 \\ \vdots \\ \omega_2 \end{bmatrix} \tag{20}$$

where both the submatrices ω_1 and ω_2 are $\mathbb{R}^{N\times 2}$, given by

$$\omega_1 = \begin{bmatrix} \frac{2}{\Delta x} & 0 \\ \frac{2}{\Delta x} & 0 \\ \vdots & \vdots \\ \frac{2}{\Delta x} & 0 \\ \frac{2}{\Delta x} & \frac{2}{\Delta y} \end{bmatrix} \quad \text{and} \quad \omega_2 = \begin{bmatrix} 0 & 0 \\ 0 & 0 \\ \vdots & \vdots \\ 0 & 0 \\ 0 & \frac{2}{\Delta y} \end{bmatrix} \tag{21}$$

The input matrix $q(t) \in \mathbb{R}^{2\times 1}$ is given by

$$q(t) = [\, q_1(t) \quad q_2(t) \,]^{\mathrm{T}} \tag{22}$$

The state Eq. (15) discretized over time intervals of length Δt is given by

$$X(k+1) = \Phi X(k) + \Gamma[q(k) + w(k)], \tag{23}$$

where

$$X(k) = [T_0(k)T_1(k)\cdots T_{M-2}(k)T_{M-1}(k)]^{\mathrm{T}}$$
$$T_0(k) = [T_{0,0}(k)T_{0,1}(k)\cdots T_{0,N-2}(k)T_{0,N-1}(k)]$$
$$T_1(k) = [T_{1,0}(k)T_{1,1}(k)\cdots T_{1,N-2}(k)T_{1,N-1}(k)]$$
$$\vdots$$
$$T_{M-1}(k) = [T_{M-1,0}(k)T_{M-1,1}(k)\cdots T_{M-1,N-2}(k)T_{M-1,N-1}(k)],$$

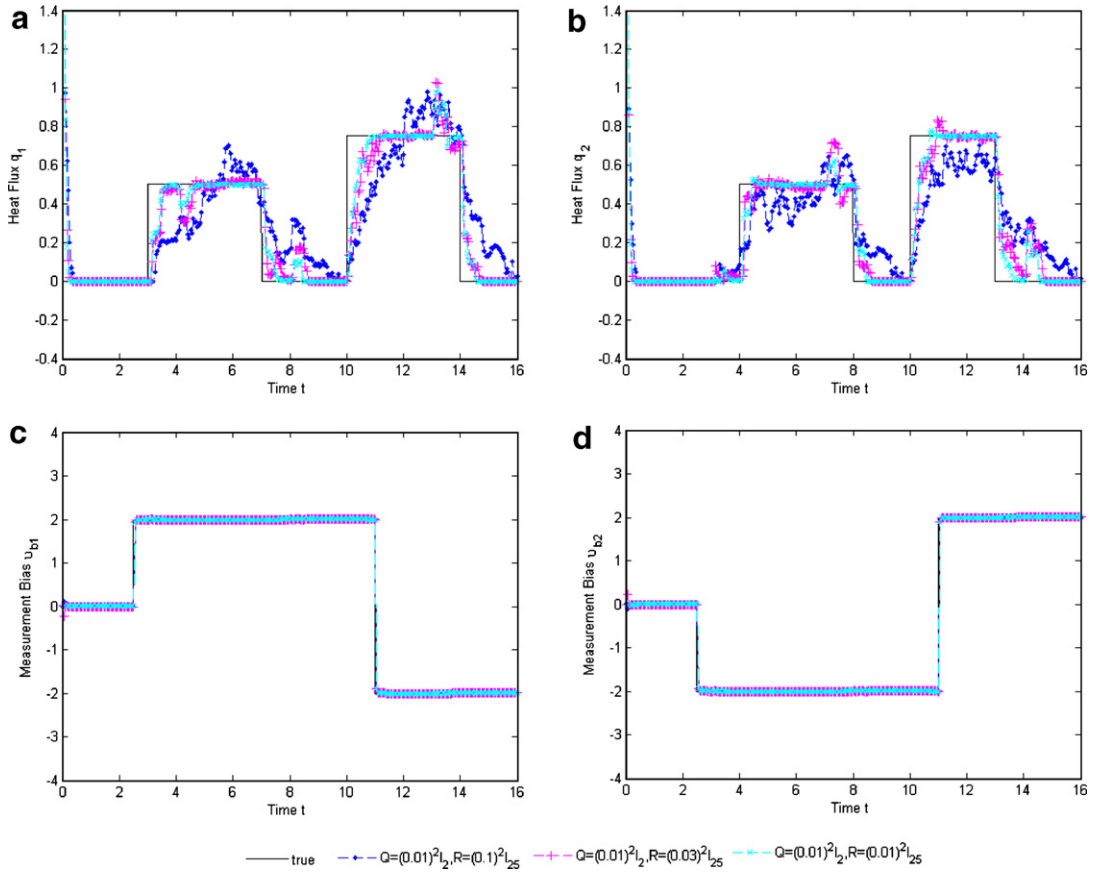

Fig. 5. Reconstructed heat fluxes and measurement biases for scenario 1. Parameters are $x_s = 0.5$, $y_s = 0.5$, $\Delta t = 0.005$, $Q_b = 0.001I_2$, $R_b = 0.001I_2$, $\alpha = 0.7$, $\theta^{(i,i)} = 0.95$, and $Pe(-1|-1) = 10^{10}I_{25}$.

$$\Phi = e^{\Psi \Delta t}$$

$$\Gamma = \int_{k\Delta T}^{(k+1)\Delta T} \exp\{\Psi[(k+1)\Delta T - \tau]\}\Omega d\tau$$

and

$$q(k) = [\, q_1(k) \quad q_2(k) \,]^{\mathrm{T}} \tag{24}$$

Here $X(k)$ represents the state vector, Φ is the state transition matrix, Γ is the input matrix, $q(k)$ is the sequence of deterministic input, and $w(k)$ is the process noise vector, assumed to be zero mean and white Gaussian with variance $E\{w(k)w^T(j)\} = Q\delta_{kj}$ and δ_{kj} is a Kronecker delta. Using Eqs. (6) and (7) and referring back to Fig. 1, the measurement equation becomes

$$Z_1(k) = T_{M-1,(N-1)/2}(k) + \upsilon_1(k) \tag{25}$$

$$Z_2(k) = T_{(M-1)/2,0}(k) + \upsilon_2(k) \tag{26}$$

or, in matrix form,

$$Z(k) = HX(k) + \upsilon(k), \tag{27}$$

where the observation vector $Z(k) = [Z_1(k)Z_2(k)]^{\mathrm{T}}$, the measurement noise vector $\upsilon(k) = [\upsilon_1(k)\upsilon_2(k)]^{\mathrm{T}}$, and the measurement matrix H is given by $\mathbb{R}^{2\times(M\times N)}$. The $\upsilon(k)$ is the measurement noise vector, assumed to be zero mean and white Gaussian. The variance of $\upsilon(k)$ is given by

$$E\{\upsilon(k)\upsilon^T(j)\} = R\delta_{kj} = \begin{bmatrix} \sigma_1^2 & 0 \\ 0 & \sigma_2^2 \end{bmatrix} \delta_{kj}, \tag{28}$$

where the matrix elements σ_1 and σ_2 represent the standard deviation of measurement noise for $\upsilon_1(k)$ and $\upsilon_2(k)$, respectively.

3. Adaptive state estimation with unknown input heat flux and measurement bias

In this section the Bayesian state estimation technique is employed for IHCP which has unknown input flux, and whose measurement sequence is corrupted with an unknown randomly switching bias in addition to white Gaussian noise. In this formulation, the input flux and bias terms are modeled as a semi-Markov process. The system analysis of semi-Markov processes is covered in depth by Howard [25]. Basically, a semi-Markov process is a discrete Markov process with finite number of states, and the time the plant spends in each state is a random variable.

We take the state equation as described in Eq. (23). The contaminated measurement equation is described as

$$Z(k+1) = HX(k+1) + \upsilon(k+1) + \upsilon_{\mathrm{b}}(k+1), \tag{29}$$

where $\upsilon_{\mathrm{b}}(k+1)$ is the measurement bias vector. Both $q(k)$ and $\upsilon_{\mathrm{b}}(k+1)$ are governed by independent semi-Markov

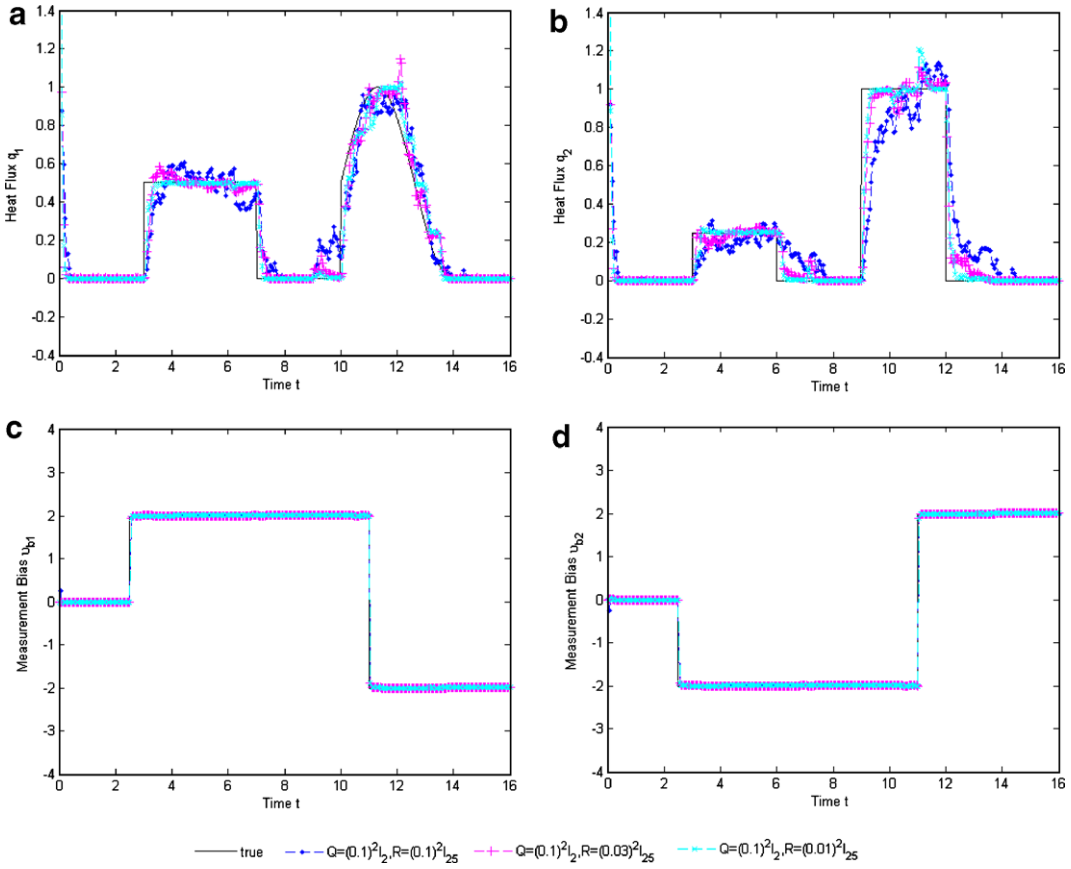

Fig. 6. Reconstructed heat fluxes and measurement biases for scenario 2. Parameters are $x_{\mathrm{s}} = 0.5$, $y_{\mathrm{s}} = 0.5$, $\Delta t = 0.005$, $Q_{\mathrm{b}} = 0.001I_2$, $R_{\mathrm{b}} = 0.001I_2$, $\alpha = 0.7$, $\theta^{(i,i)} = 0.95$, and $Pe(-1|-1) = 10^{10}I_{25}$.

processes. It is assumed that the input and bias vectors can independently take on any of the possible discrete vectors $\{q^{(1)}, \ldots, q^{(O^2)}\}$ and $\{\upsilon^{(1)}, \ldots, \upsilon^{(P^2)}\}$ for a random duration of time before a transition to a new bias occurs. Here O represents the possible discrete values of each input heat flux q_1 and q_2 and P represents the possible discrete values of each measurement bias υ_{b1} and υ_{b2}, respectively. And hence the possible combinations of q_1 and q_2 are O^2 and for υ_{b1} and υ_{b2} are P^2, respectively. The range of vectors $q^{(i)}$ $(i = 1, \ldots, O^2)$ and $\upsilon^{(j)}$ $(j = 1, \ldots, P^2)$ are modeled such that they span the entire possible ranges of $q(k)$ and $\upsilon_b(k+1)$. The optimal estimate of the state vector can be derived from the conditional mean by applying Bayesian conditional probability theory. The derivation of ASE is given in [22] and the required state estimator equations are given as

$$\hat{X}(k+1) = \sum_{i}^{O^2} \sum_{j}^{P^2} \hat{X}(k+1)^{(i,j)} W(k+1)^{(i,j)} \tag{30}$$

$$\hat{q}(k+1) = \sum_{i}^{O^2} \sum_{j}^{P^2} q^{(i)} W(k+1)^{(i,j)} \tag{31}$$

$$\hat{\upsilon}_b(k+1) = \sum_{i}^{O^2} \sum_{j}^{P^2} \upsilon^{(j)} W(k+1)^{(i,j)}, \tag{32}$$

where

$$\hat{X}(k+1)^{(i,j)} = \Phi \hat{X}(k)^{(i,j)} + \Gamma q^{(i)} + K(k+1) \times \left[Z(k+1) - \upsilon^{(j)} - H\Phi \hat{X}(k)^{(i,j)} - H\Gamma q^{(i)} \right] \tag{33}$$

and

$$M(k+1) = \Phi Pe(k) \Phi^T + \Gamma (Q + Q_b) \Gamma^T \tag{34}$$

$$K(k+1) = M(k+1) H^T [HM(k+1)H^T + R + R_b]^{-1} \tag{35}$$

$$Pe(k+1) = [I - K(k+1)H] M(k+1) \tag{36}$$

and

$$W(k+1)^{(i,j)} = C(k+1) \mathrm{e}^{-q_{ij}} \sum_{\alpha=1}^{O^2} \sum_{\beta=1}^{P^2} \theta_q^{(\alpha,i)} \theta_\upsilon^{(\beta,j)} W(k)^{(\alpha,\beta)}, \tag{37}$$

where

$$q_{ij} = \frac{1}{2} \left(Z(k+1) - \bar{z}^{(i,j)} \right)^{\mathrm{T}} [Q_z]^{-1} \left(Z(k+1) - \bar{z}^{(i,j)} \right) \tag{38}$$

with

$$\bar{z}^{(i,j)} = H\Phi \hat{X}(k)^{(i,j)} + H\Gamma q^{(i)} + \upsilon^{(j)} \tag{39}$$

$$Q_z = HM(k+1)H^T + R + R_b \tag{40}$$

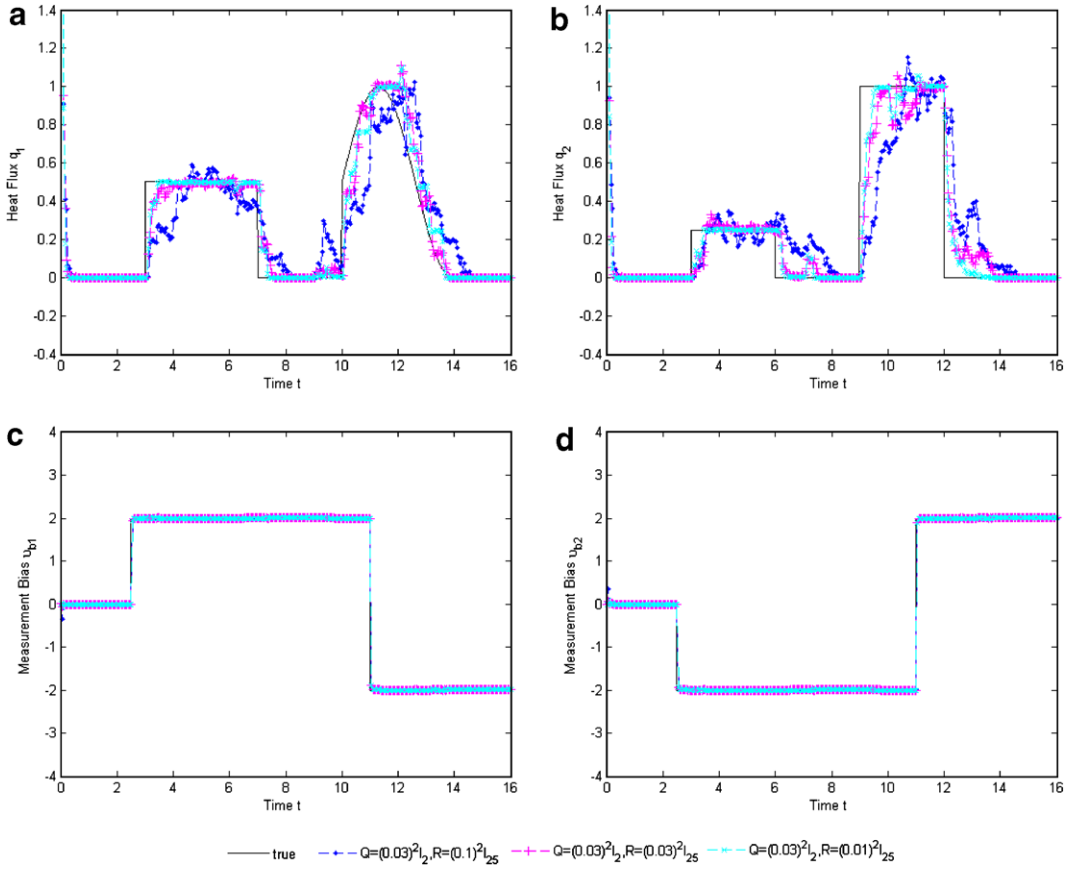

Fig. 7. Reconstructed heat fluxes and measurement biases for scenario 2. Parameters are $x_s = 0.5$, $y_s = 0.5$, $\Delta t = 0.005$, $Q_b = 0.001 I_2$, $R_b = 0.001 I_2$, $\alpha = 0.7$, $\theta^{(i,i)} = 0.95$, and $Pe(-1|-1) = 10^{10} I_{25}$.

In Eq. (30), $\hat{X}(k+1)^{(i,j)}$ is the conditional estimate of $X(k+1)$ given that $q(k+1)=q^{(i)}$ and $\upsilon_b(k+1)=\upsilon^{(j)}$ which is weighted by the probability $W(k+1)^{(i,j)}$. This probability is obtained from Eq. (37) where $\theta_q^{(\alpha,i)}$ and $\theta_\upsilon^{(\beta,j)}$ are the elements of Markov transition matrices. $C(k+1)$ is the scale factor which is determined at each iteration such that $\sum_{i=1}^{O^2}\sum_{j=1}^{P^2}W(k+1)^{(i,j)}=1$. Also, the covariance matrices R_b and Q_b compensate for additional uncertainties in the sense that $\upsilon_b(k+1)(q(k+1))$ may be between $\upsilon^{(j)}$ and $\upsilon^{(j+1)}(q^{(i)})$ and $(q^{(i+1)})$.

The block diagram of ASE is shown in Fig. 2. When the new measurement vector $Z(k+1)$ is available, the Kalman gain and covariance matrices, Eqs. (34)–(36), are computed first and are provided to different filters. Each filter differs by $q^{(i)}$ and $\upsilon^{(j)}$. A total of $O^2\times P^2$ filters exist. Each filter then calculates $\hat{X}(k+1)^{(i,j)}$ based on the predefined values of $q^{(i)}$ and $\upsilon^{(j)}$. Next, weight matrix $W(k+1)^{(i,j)}$ is calculated based on the supplied measurement vector $Z(k+1)$, previously calculated weights and supplied Markov transition matrices (Eqs. (37)–(40)). Finally, Eqs. (30)–(34) are used to give estimates of $\hat{X}(k+1)$, $\hat{q}(k+1)$ and $\hat{\upsilon}_b(k+1)$.

4. Simulations

The estimation performance of the proposed algorithm is evaluated by computer simulations by considering different types of heat fluxes and measurement biases. The coefficients Φ and Γ of the system model, for $M=5$ and $N=5$ in Eq. (23) are $\mathbb{R}^{25\times25}$ and $\mathbb{R}^{25\times2}$, respectively. The measurement matrix H in Eq. (27) is $\mathbb{R}^{2\times25}$. For the verification of the proposed algorithm, we have performed simulations on two scenarios. The unknown heat fluxes $q_1(t)$ and $q_2(t)$ which represent sudden onset and time-varying inputs, are modeled by a sequence of square and sinusoidal wave and a sequence of staggering square waves with different magnitudes. The time-varying unknown measurement biases $\upsilon_1(t)$ and $\upsilon_2(t)$ are modeled by a sequence of square waves.

In the first scenario, the settings and parameters are given as

$$q_1(t)=\begin{cases}0 & 0\leqslant t<3,7<t<10,14<t\leqslant t_f\\ 0.5 & 3\leqslant t\leqslant 7\\ 0.75 & 10\leqslant t\leqslant 14\end{cases}$$

$$q_2(t)=\begin{cases}0 & 0\leqslant t<4,8\leqslant t<10,13<t\leqslant t_f\\ 0.5 & 4\leqslant t<8\\ 0.75 & 10\leqslant t\leqslant 13\end{cases}$$

$$\upsilon_{b1}(t)=\begin{cases}0 & 0\leqslant t\leqslant 2.5\\ 2 & 2.5<t\leqslant 11\\ -2 & 11<t\leqslant t_f\end{cases}$$

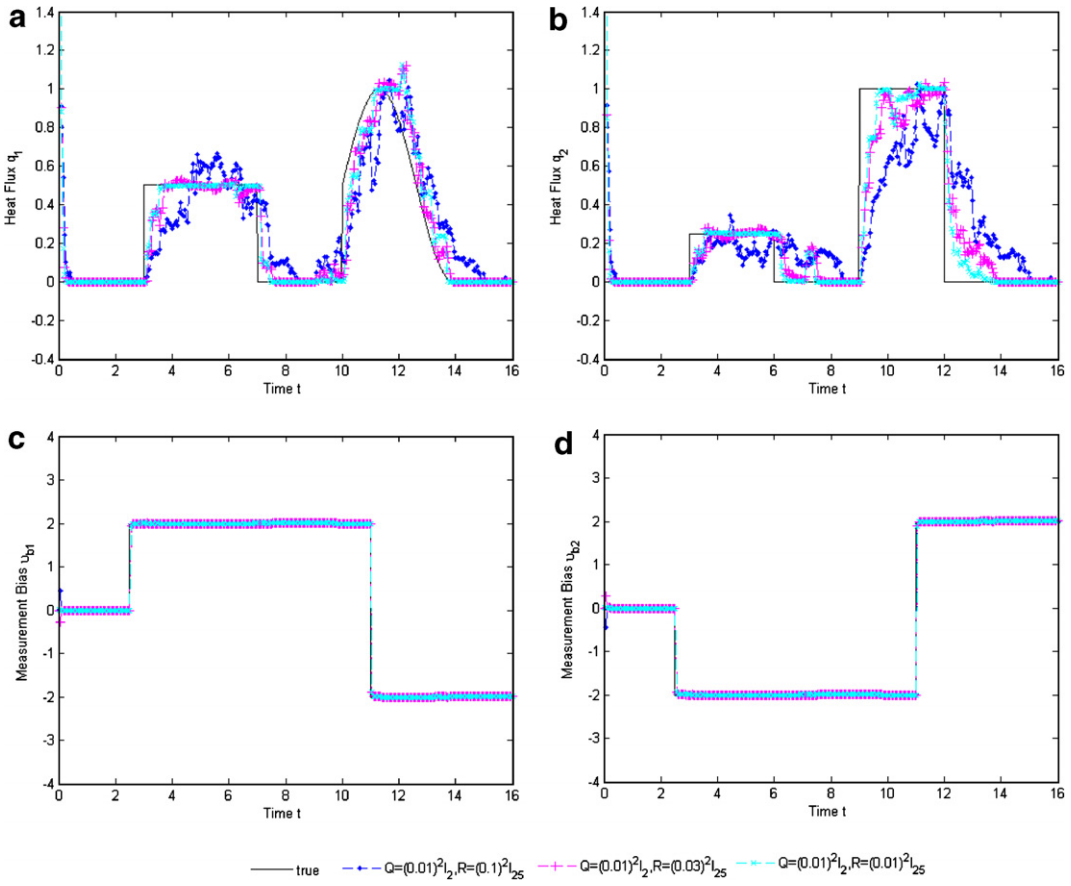

Fig. 8. Reconstructed heat fluxes and measurement biases for scenario 2. Parameters are $x_s=0.5$, $y_s=0.5$, $\Delta t=0.005$, $Q_b=0.001I_2$, $R_b=0.001I_2$, $\alpha=0.7$, $\theta^{(i,i)}=0.95$, and $Pe(-1|-1)=10^{10}I_{25}$.

$$\upsilon_{b2}(t)=\begin{cases}0 & 0\leqslant t\leqslant 2.5\\ -2 & 2.5<t\leqslant 11\\ 2 & 11<t\leqslant t_f\end{cases}$$

In the scenario 2, the settings and parameters are given as

$$q_1(t)=\begin{cases}0 & 0\leqslant t<3,7<t<10,14<t\leqslant t_f\\ 0.5 & 3\leqslant t\leqslant 7\\ 0.5[1+\sin\mu(t-10)] & 10\leqslant t\leqslant 14\end{cases}$$

$$q_2(t)=\begin{cases}0 & 0\leqslant t<3,6<t<9,12<t\leqslant t_f\\ 0.25 & 3\leqslant t\leqslant 6\\ 1 & 9\leqslant t\leqslant 12\end{cases}$$

$$\upsilon_{b1}(t)=\begin{cases}0 & 0\leqslant t\leqslant 2.5\\ 2 & 2.5<t\leqslant 11\\ -2 & 11<t\leqslant t_f\end{cases}$$

$$\upsilon_{b2}(t)=\begin{cases}0 & 0\leqslant t\leqslant 2.5\\ -2 & 2.5<t\leqslant 11\\ 2 & 11<t\leqslant t_f\end{cases}$$

In all the simulations, the sensor locations are $(\frac{x_s}{2},0)$ and $(x_s,\frac{y_s}{2})$, $\mu=1.2$, $t=k\Delta t$ and final time $t_f=16$.

In the ASE, it is assumed that the initial values for the weighting terms are all equal, i.e., $W(0)^{(i,j)}=1_{O^2\times P^2}$. The values of the Markov transition matrices, assumed as

$$\theta_q^{(i,j)}=\frac{(1-0.95)}{(1-O^2)},\quad (i\neq j)$$

$$\theta_q^{(ii)}=0.95$$

$$\theta_\upsilon^{(i,j)}=\frac{(1-0.95)}{(1-P^2)},\quad (i\neq j)$$

$$\theta_\upsilon^{(ii)}=0.95$$

based on Moose et al. [22,24], were used in most of the simulations. In the simulations, we have assumed $\theta_q^{(i,i)}=\theta_\upsilon^{(i,i)}=\theta^{(i,i)}$, i.e., the diagonals of Markov transition matrices are similar for both input heat fluxes and measurement sensor biases.

Also, in order to reduce the effect of noise on the weighting terms, a first-order low-pass filter was used as $W(k+1)^{(i,j)}=(\alpha)W(k)^{(i,j)}+(1-\alpha)\widetilde{W}(k)^{(i,j)}$, where $\widetilde{W}(k)^{(i,j)}$ are the weights as calculated from Eq. (37). The range of $q^{(i)}$ for both input heat fluxes is $\{0,0.25,0.5,0.75,1,1.25\}$ and the range of $\upsilon^{(j)}$ for both sensor biases is $\{-2,0,2\}$, i.e., $O=6$ and $P=3$, respectively.

The simulation results with variation of process and measurement noise for both scenarios are shown in Figs. 3–8. The process and measurement noises of standard deviations 0.1, 0.03 and 0.01 are considered. In scenario 2, the heat flux q_1 consists of a square wave and a sinosidal wave whereas the heat flux q_2 consists of two square waves. The

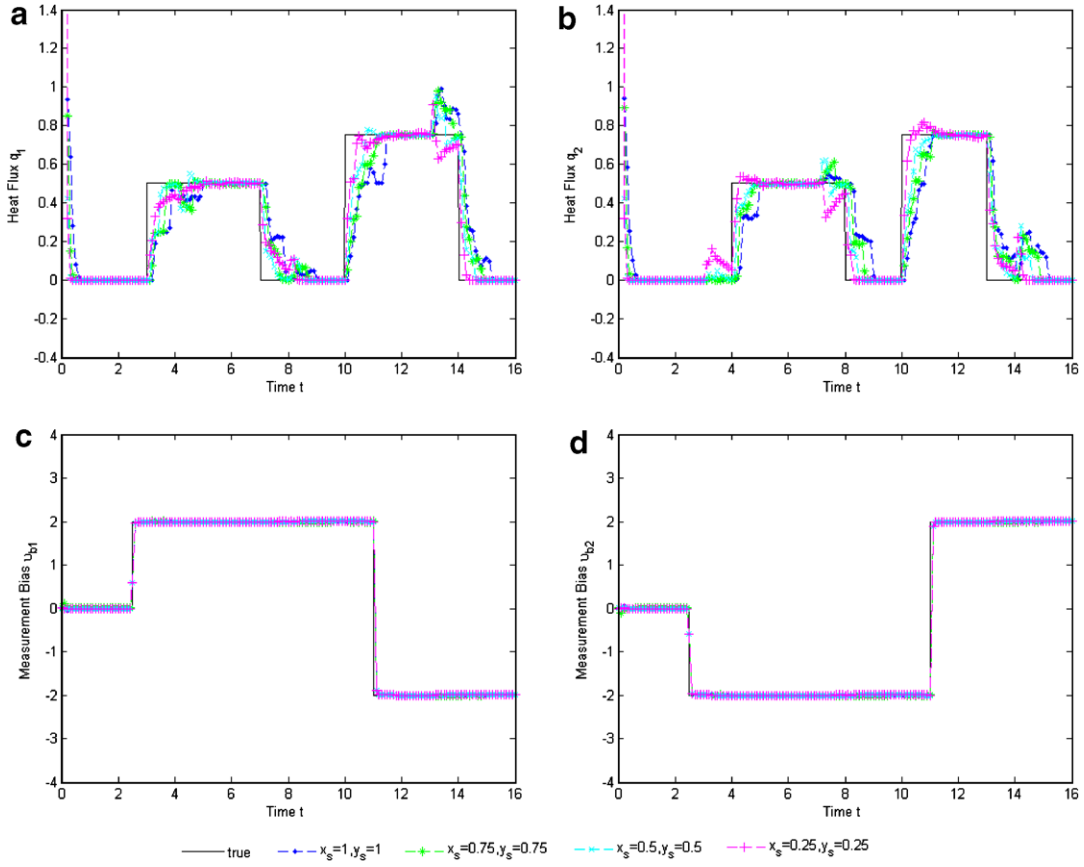

Fig. 9. Reconstructed heat fluxes and measurement biases for scenario 1. Parameters are $\Delta t=0.01$, $Q=(0.01)^2I_2$, $R=(0.01)^2I_{25}$, $Q_b=0.001I_2$, $R_b=0.001I_2$, $\alpha=0.7$, $\theta^{(i,i)}=0.95$, and $Pe(-1|-1)=10^{10}I_{25}$.

reason behind taking the sinosidal wave is that since q and υ_b can take on O^2 and P^2 possible discrete values, therefore, if the values lie between $q^{(i)}$ and $q^{(i+1)}$ and $\upsilon^{(j)}$ and $\upsilon^{(j+1)}$, respectively, then ASE should be able to estimate well between these ranges. In the context of scenario 1 notice abrupt changes at time steps $t = 2.5, 3, 4, 7, 8, 10, 11, 13, 14$ for true values of input heat fluxes and measurement sensor biases. These are the trouble points at which some unexpected peaks are prominent for reconstruction results of input heat fluxes. Since the state estimation, input heat flux estimation and measurement sensor bias estimation all depend on the single weight matrix, therefore, when there is a sudden and abrupt shift in the values, the estimator needs a little time to converge. Hence, interdependence in estimation of different variables leads to unwanted peaks when there are abrupt changes. The same phenomenon can be observed for scenario 2 at time steps $t = 2.5, 3, 6, 7, 9, 10, 11, 12$. By extensive simulations, we reached the conclusion that at least one of the unknowns will be estimated better than the others when using ASE, hence in the simulations, the measurement sensor biases were estimated well i.e., the estimated values are nearly similar to true values whereas the input heat fluxes estimation show some discrepancies between the estimated and true values. It should also be noted that the estimation performance is affected more by higher process and measurement noise levels and so in Figs. 3–8 when the standard deviation of process and measurement noise is 0.1, many fluctuations can be observed in the estimated heat fluxes. However, the performance improves when the process and measurement noise is reduced, i.e., with standard deviation of 0.03 and 0.01, respectively.

The ASE is an online estimator and the estimated heat flux may present some time lag which is dependent on the size of the region and location of the measurement sensor. Fig. 9 shows the reconstruction results with different region sizes. It can be noticed that with a smaller region, i.e., when $x_s = 0.25, y_s = 0.25$, the lag is smaller in comparison to the region with larger size, i.e., when $x_s = 1, y_s = 1$. To see the effect of sampling time on the stability of the algorithm, the reconstruction results with varying sampling times are shown in Fig. 10. Here, it should be noted that for a big sampling time, the online estimator has a big transient period in the start, for example, when $\Delta t = 0.1$. For $\Delta t = 0.001$, the transient period is significantly small. It can also be noticed that with a very small sampling time, on the average, the estimation performance is better, however, the unwanted peaks can also be observed, for example, with $\Delta t = 0.001$ and $\Delta t = 0.005$. Facing the same problem, Moose et al. [22] suggested to use the first-order low-pass filter to reduce the effect of noise on the weight matrix. By incorporating the first-order low-pass filter,

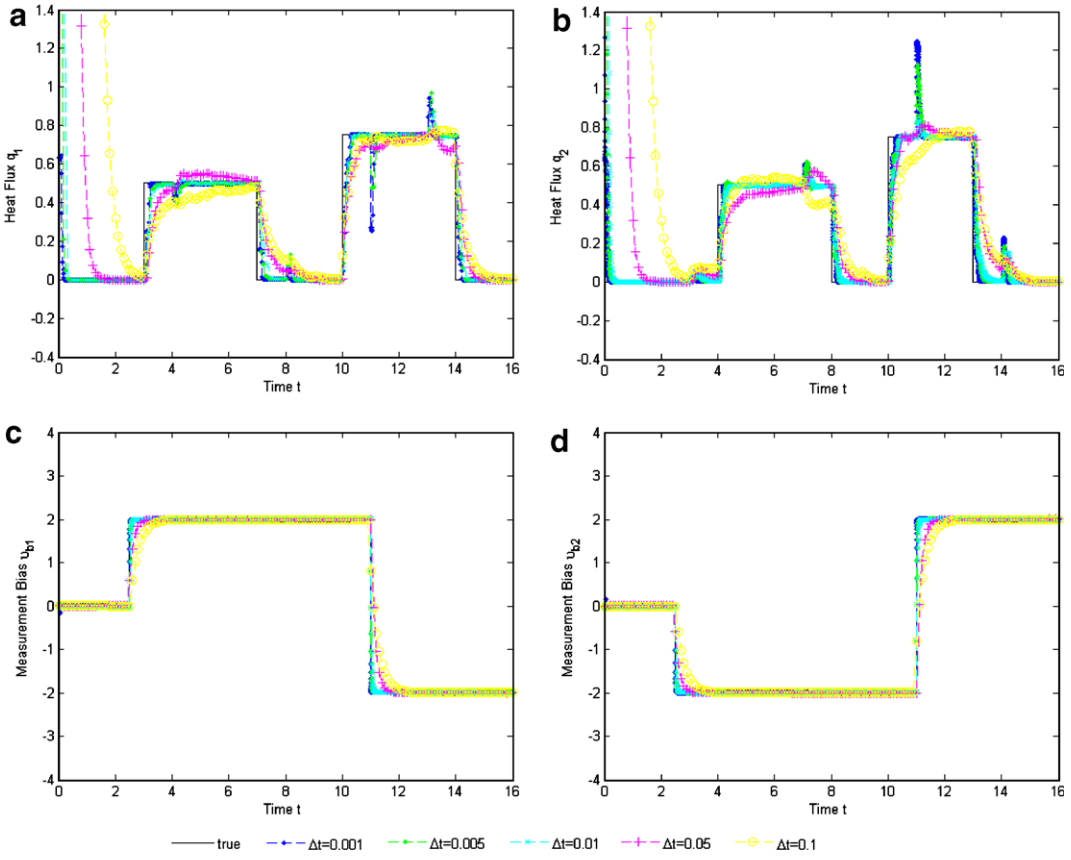

Fig. 10. Reconstructed heat fluxes and measurement biases for scenario 1. Parameters are $x_s = 0.5$, $y_s = 0.5$, $Q = (0.1)^2 I_2$, $R = (0.01)^2 I_{25}$, $Q_b = 0.001 I_2$, $R_b = 0.001 I_2$, $\alpha = 0.7$, $\theta^{(i,i)} = 0.95$, and $Pe(-1|-1) = 10^{10} I_{25}$.

we are able to reduce the duration of peaks to certain extent. The reconstruction results with different values of α for the low-pass filter are shown in Fig. 11. It is observed that with the higher values of α, the peaks are smaller. However, higher values of α also result in an increase in the transient period in the start and introduce time lag. In the considered scenarios, $\alpha = 0.7$ offers a good trade-off between peak reduction and estimation performance. An analysis of time lag has already been done by Scarpa et al. [2] which introduces future time measurements in Kalman algorithm. An extension of this technique to include future measurements would be an interesting topic for future research.

Finally, the effect of Markovian transition probabilities are considered in Fig. 12. A higher value of $\theta^{(i,i)} = 0.95$ for both input heat fluxes and measurement biases gives optimum performance. In ASE, the Kalman gain and the required covariances for multiple filters are pre-calculated and stored once per every iteration (measurement data acquisition) to reduce the computational burden of ASE. Summing up our findings, the performance of the ASE depends heavily on the

- process noise, measurement noise along with choice of Q_b and R_b.
- changes in the input heat flux and measurement sensor bias between subsequent iterations whether the changes are abrupt changes or smooth changes.
- the number of filters used, i.e., range of q and υ_b.
- the number of unknowns to be estimated. Since all the estimates depend on a single weight matrix, therefore, with less unknown, the results are going to be more accurate.
- the Markov transition matrix used to specify the probability measure given to each filter.
- first-order low-pass filter used to reduce the effect of noise on weight matrix for reduction of unwanted peaks.

5. Conclusions

In this paper, we have presented adaptive state estimator for the estimation of input heat flux and measurement sensor bias in two-dimensional inverse heat conduction problems. The algorithm is implemented by a parallel bank of Kalman-type estimators, each matched to a set of different possible input fluxes and biases. The measurement sequence, after being processed in each filter, is weighted according to a specific probability measure, and then summed to give a final estimate of the state, the input heat flux and the measurement bias. Simulations for the system

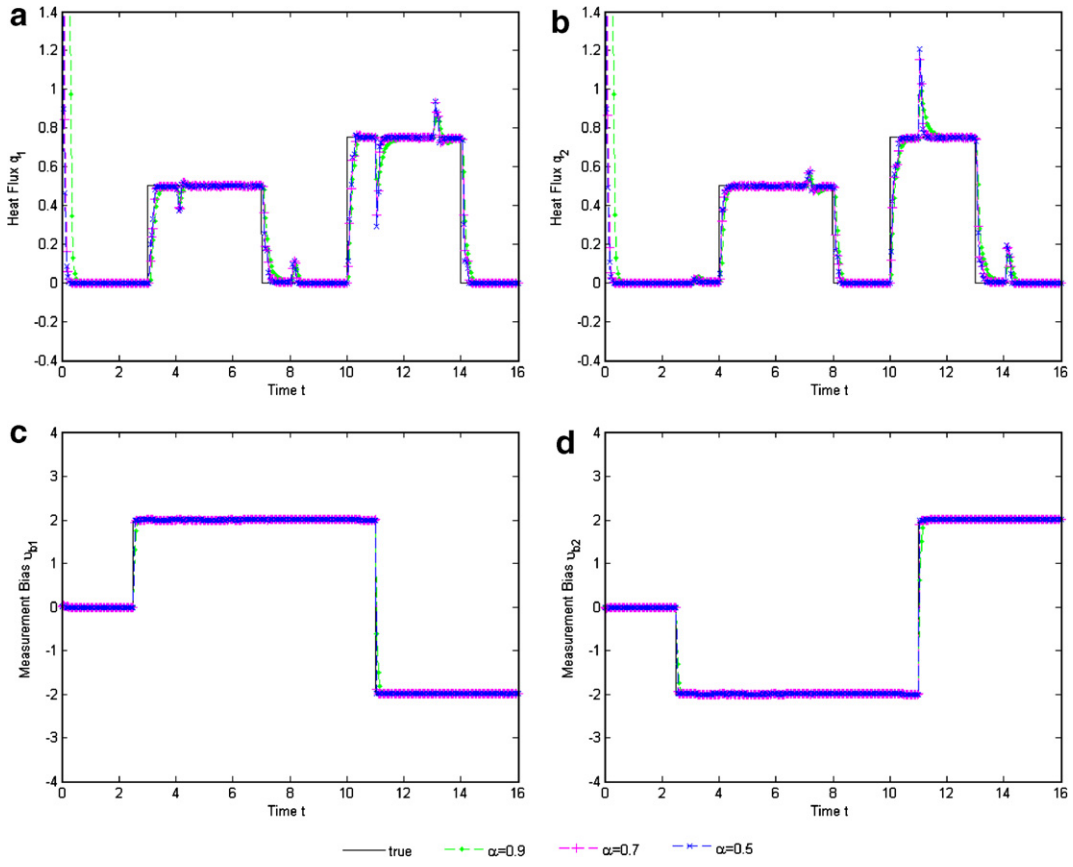

Fig. 11. Reconstructed heat fluxes and measurement biases for scenario 1. Parameters are $x_s = 0.5$, $y_s = 0.5$, $\Delta t = 0.005$, $Q = (0.01)^2 I_2$, $R = (0.01)^2 I_{25}$, $Q_b = 0.001 I_2$, $R_b = 0.001 I_2$, $\theta^{(i,i)} = 0.95$, and $Pe(-1|-1) = 10^{10} I_{25}$.

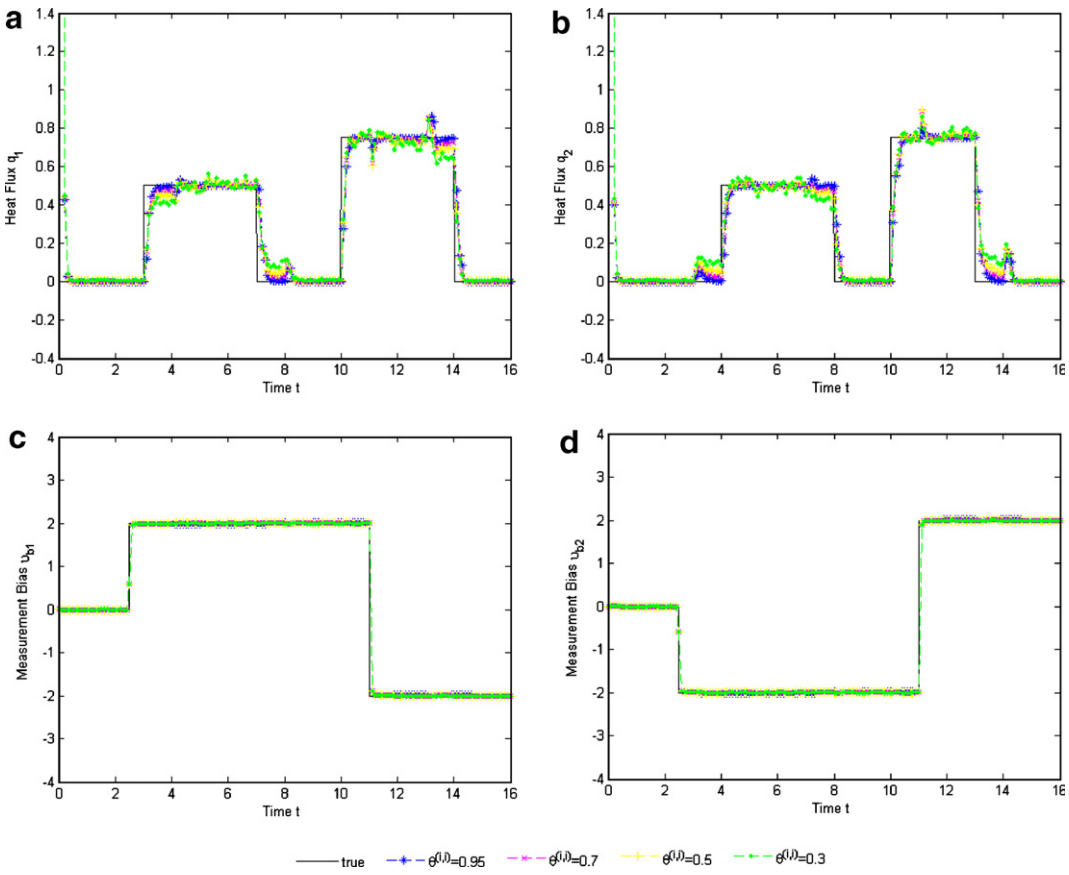

Fig. 12. Reconstructed heat fluxes and measurement biases for scenario 1. Parameters are $x_s = 0.5$, $y_s = 0.5$, $\Delta t = 0.005$, $Q = (0.01)^2 I_2$, $R = (0.01)^2 I_{25}$, $Q_b = 0.001 I_2$, $R_b = 0.001 I_2$, $\alpha = 0.7$, and $Pe(-1|-1) = 10^{10} I_{25}$.

was presented under different scenarios to test the compatibility of the proposed algorithm.

Acknowledgements

This work is supported by IITA's ITSP. The part of researchers participating in this study are supported by the grant from "the 2nd phase BK21 project".

References

[1] S. Kim, B.J. Jung, M.C. Kim, K.Y. Kim, A note on the direct estimation of thermal properties in a transient nonlinear heat conduction medium, Int. Commun. Heat Mass Transfer 29 (6) (2002) 735–1933.
[2] F. Scarpa, G. Milano, Kalman smoothing technique applied to the inverse heat conduction problem, Numer. Heat Transfer Part B 28 (1995) 79–96.
[3] J. Kaipio, E. Somersalo, Nonstationary inverse problems and state estimation, J. Inverse Ill-Posed Problems 7 (1999) 273–282.
[4] P.C. Tuan, C.C. Ji, L.W. Fong, W.T. Huang, An input estimation approach to on-line two-dimensional inverse heat conduction problems, Numer. Heat Transfer Part B 29 (1996) 345–363.
[5] P.C. Tuan, L.W. Fong, W.T. Huang, Application of Kalman filtering with input estimation technique to on-line cylindrical inverse heat conduction problems, JSME Int. J. Ser. B 40 (1) (1997) 126–133.
[6] P.C. Tuan, S.C. Lee, W.T. Hou, An efficient on-line thermal input estimation method using Kalman filter and recursive least square algorithm, Inverse Problem Eng. 5 (1997) 309–333.
[7] P.C. Tuan, W.T. Hou, The adaptive robust weighting input estimation method for 1-D inverse heat conduction problem, Numer. Heat Transfer Part B 34 (1998) 439–456.
[8] P.C. Tuan, M.C. Ju, Adaptive weighting input estimation algorithm for one dimensional cylindrical heat conduction problems, Proc. Natl. Sci. Counc. ROC(A) 25 (3) (2001) 163–171.
[9] P.C. Tuan, T.C. Chen, Input estimation method including finite element scheme for solving inverse heat conduction problems, Numer. Heat Transfer Part B 47 (3) (2005) 277–290.
[10] C.-C. Ji, P.-C. Tuan, H.-Y. Jang, A recursive least-squares algorithm for on-line 1-D inverse heat conduction estimation, Int. J. Heat Mass Transfer 40 (9) (1997) 2081–2096.
[11] P.C. Tuan, L.W. Fong, An IMM tracking algorithm with input estimation, Int. J. Sys. Sci. 27 (7) (1996) 620–639.
[12] H.Y. Jang, P.C. Tuan, T.C. Chen, T.S. Chen, Input estimation method combined with the finite-element scheme to solve IHCP hollow-cylinder inverse heat conduction problems, Numer. Heat Transfer Part A 50 (3) (2006) 263–280.
[13] H.M. Park, W.S. Jung, On the solution of multidimensional inverse heat conduction problems using an efficient sequential method, ASME J. Heat Transfer 123 (2001) 1021–1029.
[14] N. Daouas, M.S. Rahouani, Version étendue du filtre de Kalman discret appliquée à un probléme inverse de conduction de chaleur non linéaire, Int. J. Therm. Sci. 39 (2000) 191–212.
[15] N. Daouas, M.S. Rahouani, A new approach of the Kalman filter using future temperature measurements for nonlinear inverse heat conduction problems, Numer. Heat Transfer Part B 45 (2004) 565–585.

[16] H.M. Wang, T.C. Chen, P.C. Tuan, S.G. Den, Adaptive-weighting input estimation approach to nonlinear inverse heat-conduction problems, J. Thermophys. Heat Transfer 19 (2) (2005) 209–216.
[17] F. Scarpa, G. Milano, Influence of sensor calibration uncertainties in the inverse heat conduction problem(IHCP), Numer. Heat Transfer Part B: Fundamentals 36 (4) (1999) 457–474.
[18] J. Wang, N. Zabaras, A bayesian inference approach to the stochastic inverse heat conduction problem, Int. J. Heat Mass Transfer 47 (2004) 3927–3941.
[19] J. Wang, N. Zabaras, Hierarchical bayesian models for inverse problems in heat conduction, Inverse Probl. 21 (2005) 183–206.
[20] J. Wang, N. Zabaras, Using bayesian statistics in estimation of heat source in radiation, Int. J. Heat Mass Transfer 48 (2005) 15–29.
[21] J. Wang, N. Zabaras, A markov random field model of contamination source identification in porous media flow, Int. J. Heat Mass Transfer 49 (2006) 939–950.
[22] R.L. Moose, M.K. Sistanizadeh, G. Skagfjord, Adaptive state estimation for a system with unknown input and measurement bias, IEEE Trans. Ocean Eng. 12 (1987) 222–227.
[23] K.Y. Kim, B.S. Kim, H.C. Kim, M.C. Kim, K.Y. Lee, B.J. Chung, S. Kim, Inverse estimation of time-dependent boundary heat flux with an adaptive input estimator, Int. Commun. Heat Mass Transfer 30 (2003) 475–484.
[24] R.L. Moose, M.K. Sistanizadeh, G. Skagfjord, Adaptive estimation for a system with unknown measurement bias, IEEE Trans. Aero. Electron. Sys. 22 (1986) 732–739.
[25] R.A. Howard, System analysis of semi-Markov processes, IEEE Transs. Mil. Electron. MIL-8 (1964) 114–124.
[26] A.H. Jazwinski, Stochastic Processes and Filtering Theory, Academic Press, New York, 1970.
[27] J.M. Mendel, Lessons in Digital Estimation Theory, Prentice-Hall, Englewood Cliffs, NJ, 1987.